Impact of the Neighbor's Order on the Capacity of Millimeter-Wave Links with Poisson-Distributed Nodes in Line of Sight Conditions

M. Comisso, F. Vatta, G. Buttazzoni, and F. Babich
Department of Engineering and Architecture, University of Trieste, Italy,
E-mail: {mcomisso,vatta,gbuttazzoni,babich}@units.it

***Abstract*— This paper presents a theoretical model for investigating the average capacity of a millimeter wave (mmWave) communication link in line of sight conditions, when a fixed binary phase-shift keying (BPSK) or a quadrature PSK (QPSK) modulation is used and the nodes are distributed according to a homogeneous Poisson point process (PPP). In particular, as compared to the existing PPP approaches, which often consider the sole nearest neighbor as a possible destination, the proposed analysis enables to evaluate the link performance for a neighbor of any order, thus providing a more complete view of the achievable capacity. Besides, the adoption of the BPSK/QPSK modulations helps to obtain a more realistic estimation with respect to the ideal one provided by the usually adopted Shannon bound. Moreover, the derived formulas, which are expressed in analytical form and checked by extensive simulations, include the influence of all the main mmWave propagation phenomena: path-loss attenuation, small- and mid-scale fading. The developed model is specifically exploited to explore the impact of the average cell radius and of the selected frequency band on the sustainability of the mmWave link as the destination becomes farther from the source.**

***Index Terms*— Transmission capacity; millimeter-waves; neighbor distribution; line of sight.**

I. Introduction

The ongoing deployment of the fifth-generation (5G) system is at present mainly focused on the implementation of the architecture and on the testing of the added virtual functionalities [1]. Novel radio components have been also installed, but, at this stage, mainly considering the 3.7 GHz band, rather than the more challenging millimeter wave (mmWave) ones. This second step, which will lead to the actual 5G, is expected to be accomplished in the next years [2]. In fact, together with node densification [3–6], and massive multiple input multiple output [7–9], mmWaves identify the big-three elements of the 5G technology for the provisioning of low-latency ultra-high capacity services [10–12]. This depicts a situation in which several devices, such as user equipments, sensors, and actuators, simultaneously exchange information with a base station or on a peer-to-peer basis [13–15].

The resulting scenario has been deeply analyzed in many relevant studies [16–20]. These works cover several aspects of mmWave communication and networking, including the impact of interference [16], densification [17], node position [18], multi-tiring [19], and initial access [20], through elaborated mathematical frameworks. A common hypothesis assumed in all these models concerns the usage of a uniform distribution or of a homogeneous Poisson point process (PPP) to identify the location of the nodes, usually considering a unique statistic to describe the position of a destination or of an interferer with respect to a given source. More precisely, when the PPP model is adopted, the analyses are commonly developed considering the nearest neighbor assumption, that is, taking into account just the node closest to the source. This approach has the advantage of leading to more tractable models, but its accuracy is guaranteed as long as the nearest neighbor actually represents the intended destination or the most harmful interferer. However, in realistic 5G scenarios characterized by mobility, both these assumptions may not hold, since the destination might not coincide with the closest node or the closest interferer might not be the most powerful one, because of the statistical channel fluctuations. An analysis including the neighbor of any order may be hence desirable to better understand the 5G link performance.

To address this issue, this paper proposes a theoretical model for evaluating the capacity of a mmWave line of sight (LoS) link in the presence of binary phase-shift keying (BPSK) and quadrature PSK (QPSK) modulations when the nodes are located according to a homogeneous PPP. Differently from the existing strategies, which rely on the nearest neighbor approximation, the presented model considers a neighbor of generic order to characterize the link performance also for statistically distant destinations. Furthermore, the usage of the BPSK/QPSK modulations provides more practical results as compared to those achievable using the ideal Shannon limit. All the obtained expressions, whose accuracy is checked by extensive Monte Carlo simulations, are calculated in analytical form, thus making easier their implementation. The main contribution of the proposed mathematical analysis, which includes path-loss attenuation, small- and mid-scale fading, consists in enabling the calculation of the link performance for both close and distant neighbors as a function of the average cell radius and of the chosen mmWave band.

The paper is organized as follows. Section II describes the analyzed scenario. Section III illustrates the theoretical model. Section IV presents the analytical and simulation results. Section V remarks the main conclusions.

[1]This work is partly supported by the Italian Ministry of University and Research within project FRA 2021 (Univ. of Trieste, Italy) "Interference modeling in ultra-dense 5G/6G networks."

Notation. Throughout the paper the following notation is used: $\mathbb{N}_{>0}$ denotes the set of positive integers; $\mathbb{R}_{>0}$ and $\mathbb{R}_{\geq 0}$ denote the sets of positive and non-negative reals, respectively; $\mathbf{E}[X]$ denotes the expectation of a random variable (r.v.) X; $\mathbb{1}_{\mathbf{X}}(\mathbf{x})$ denotes the indicator function (i.e., $\mathbb{1}_{\mathbf{X}}(\mathbf{x})=1$ if $\mathbf{x}\in\mathbf{X}$, $\mathbb{1}_{\mathbf{X}}(\mathbf{x})=0$ if $\mathbf{x}\notin\mathbf{X}$); $\Gamma(a)$ denotes the gamma function; $\Gamma(a;x)$ and $\gamma(a;x)$ denote the upper and the lower incomplete gamma functions, respectively; ${}_2F_1(a_1,a_2;b;x)$ denotes the hypergeometric function.

II. Scenario

The analyzed scenario is identified by a mmWave network where the nodes are located on the bi-dimensional $\mathbb{R}^2$ space according to a spatial homogeneous PPP of intensity λ. In this scenario, consider the communication between two nodes: a source S and a destination. Since $\mathbb{R}^2$ is an infinite space, assume, without loss of generality, that S lies at the center of this space. The possible location of the destination with respect to S can be statistically modeled by considering all the k-th neighbors D_k for $k\in\mathbb{N}_{>0}$, where $k=1$ identifies the nearest neighbor, $k=2$ identifies the second nearest neighbor, and so on. Thus, in general, k denotes the neighbor's order. The distance between S and D_k can be hence described by a r.v. R_k, whose probability density function (pdf) have been derived in [21] as:

$$f_{R_k}(r)=\frac{2\pi^k\lambda^k}{\Gamma(k)}\,r^{2k-1}\exp\left(-\pi\lambda r^2\right)\mathbb{1}_{\mathbb{R}_{\geq 0}}(r),\ k\in\mathbb{N}_{>0}. \quad (1)$$

The cumulative density function (cdf) of R_k can be immediately determined by integrating (1) on r, hence obtaining:

$$\begin{aligned}F_{R_k}(r)&=\int_{-\infty}^{r}f_{R_k}(r')\mathrm{d}r'\\&=\frac{\gamma(k;\pi\lambda r^2)}{\Gamma(k)}\,\mathbb{1}_{\mathbb{R}_{\geq 0}}(r),\ k\in\mathbb{N}_{>0}.\end{aligned} \quad (2)$$

The adoption of (2) for modeling the $\mathrm{S}-\mathrm{D}_k$ distance enables to consider, beside the usually analyzed nearest neighbor case, a set of further situations in which the destination does not lie close to its desired source. These situations may occur, for example, in mobile scenarios with time delivery constraints, where the nodes are not allowed to wait for an advantageous topology configuration to attempt the communication [22]. In these realistic cases, it is very likely that the closest node does not represent the intended source or destination.

Concerning the propagation environment, several studies have identified three possible link states for a mmWave link: LoS, when S and D_k are in optical visibility; Non-LoS (NLoS), when S and D_k are not in optical visibility, but they may be however able to exchange information; and, finally, outage (OUT), when the communication is impossible due to the complete obstruction of the link. Within these three states, the LoS one leads to the best performance, thus clearly putting into evidence the benefits of the mmWave systems with respect to the existing microwave ones. Therefore, to properly explore the achievable channel capacity of a mmWave network, we focus on the LoS case, which may be viewed as an upper bound for the derived performance figures. Several measurement campaigns have revealed that the mmWave channel is mainly affected by path-loss attenuation and mid-scale fading, but small-scale fading should be also considered when the influence of the path amplitude gains over a local area must be estimated [23]. For this motivation, all the three phenomena (path-loss, shadowing, and fading) are taken into account. To this regard, it is worth to remark that, even in LoS conditions, mid-scale fading effects have to be included. This might seem somewhat counterintuitive, since, in a LoS environment, the direct $\mathrm{S}-\mathrm{D}_k$ visibility should remove the possibility that obstacles, leading to shadowing, result present. Instead, the occurrence of this event cannot be excluded, since the optical visibility ensured by the LoS condition does not directly imply the more stringent radio visibility, characterized by a completely unobstructed first Fresnel zone. When optical visibility is guaranteed, obstacles partly shadowing the radio signal might be anyway present, thus mid-scale fading should be taken into account also in a LoS environment.

According to the considered propagagation scenario, the omnidirectional path-loss attenuation is modeled as a function of the r.v. R_k as [24]:

$$L(R_k)=\frac{1}{\alpha R_k^{\nu}}, \quad (3)$$

where α denotes the floating intercept and $\nu=2$ represents the average path-loss exponent in LoS conditions. The specific values for the (α,ν) pair have been derived, firstly, by extensive measurement campaigns in the 28 and 73 GHz mmWave bands and, subsequently, by statistical analyses of the acquired data. A similar approach has been adopted to characterize mid-scale fading, which is modeled by a r.v. Ξ having a log-normal distribution and hence described by a pdf:

$$f_{\Xi}(\xi)=\frac{1}{\sqrt{2\pi}\sigma\xi}\exp\left(-\frac{\log^2\xi}{2\sigma^2}\right)\mathbb{1}_{\mathbb{R}_{>0}}(\xi), \quad (4)$$

where σ identifies the shadowing standard deviation. For small-scale fading, measurements in the mmWave channel have been carried out using a Rice distribution [23], which may be however properly approximated by the Nakagami one for the purpose of achieving tractable analytical expressions during the possible integral operations. Accordingly, fading is modeled adopting a gamma distributed r.v. Ψ having pdf:

$$f_{\Psi}(\psi)=\frac{m^m}{\Gamma(m)}\,\psi^{m-1}\exp\left(-m\psi\right)\,\mathbb{1}_{\mathbb{R}_{\geq 0}}(\psi), \quad (5)$$

where $m(\geq 1/2)$ represents the Nakagami parameter. The further quantity included in the considered mmWave propagation environment is the noise power, which is assumed constant and given by [19]:

$$\mathcal{N}=\mathcal{N}_0\cdot W\cdot\mathcal{F}, \quad (6)$$

where $\mathcal{N}_0\cong 3.98\cdot 10^{-21}$ W/Hz denotes the noise spectral density, W identifies the available bandwidth, and $\mathcal{F}$ represents the noise figure of the mmWave receiver.

The latter fundamental element required to evaluate the capacity $\mathcal{C}$ of a mmWave communication is the modulation scheme. To this regard, the Shannon bound is often adopted to describe the relationship between $\mathcal{C}$ and the Signal to Noise Ratio (SNR) Υ. This choice is useful when the objective is

the derivation of the ideal performance in the presence of a perfectly adaptive system, but, when a more practical situation is of interest, it may become too optimistic. In this second case, the possibility of evaluating the capacity in the presence of a fixed linear modulation would lead to more realistic results. For this reason, this study relates the SNR to the capacity by exploiting the expression derived in [25]:

$$C(\Upsilon) = h - h\exp\left[-\varsigma_1\left(\frac{\Upsilon}{h}\right)^{\varsigma_2} + \varsigma_3\right],\ h = 1, 2, \quad (7)$$

which holds for BPSK ($h = 1$) and QPSK ($h = 2$) modulations, and where $\varsigma_1 \cong 1.2860$, $\varsigma_2 \cong 0.9308$, $\varsigma_3 \cong 0.0102$ are suitable parameters. The formula given by (7) is an approximation of the exact capacity, which, however, is very accurate, since the error remains lower than 1% as long as the SNR results not too close to zero.

III. Analysis

According to the above described propagation scenario and the chosen system parameters, this section presents the analytical model necessary to derive the cdf of the SNR and the corresponding average capacity.

A. SNR statistic

The analysis developed to obtain the SNR statistic is carried out in four steps. Firstly, the influence of the path-loss attenuation is taken into account. Secondly, the effect of small-scale fading is added. The third step aims to evaluate the impact of shadowing, while the fourth and final step derives the statistic of the SNR.

Lets start with the first step. To this aim, define the r.v. T_k, representing the power received by D_k from S in the absence of shadowing and fading. By recalling (3) for the LoS case ($\nu = 2$), this r.v. can be expressed as:

$$T_k = P_{\mathrm{S}} G_{\mathrm{S}} G_{\mathrm{D}} L(R_k) = \frac{P_{\mathrm{S}} G_{\mathrm{S}} G_{\mathrm{D}}}{\alpha R_k^2} = \frac{\varpi}{R_k^2},\ k \in \mathbb{N}_{>0}, \quad (8)$$

where P_{S} denotes the power transmitted by S, G_{S} represents the transmitting antenna gain of S, G_{D} identifies the receiving antenna gain of D_k (assumed identical for all $k \in \mathbb{N}_{>0}$), and:

$$\varpi = \frac{P_{\mathrm{S}} G_{\mathrm{S}} G_{\mathrm{D}}}{\alpha}. \quad (9)$$

By inverting (8) with respect to R_k and remembering (2) to model the location of the k-th neighbor, the cdf of T_k can be obtained as:

$$\begin{aligned} F_{T_k}(t) &= \Pr\{T_k \le t\} = \Pr\left\{\frac{\varpi}{R_k^2} \le t\right\} \\ &= 1 - \Pr\left\{R_k < \sqrt{\frac{\varpi}{t}}\right\} = 1 - F_{R_k}\left(\sqrt{\frac{\varpi}{t}}\right) \\ &= \frac{1}{\Gamma(k)}\,\Gamma\left(k; \frac{\varphi}{t}\right)\ \mathbb{1}_{\mathbb{R}_{>0}}(t),\ k \in \mathbb{N}_{>0}, \end{aligned} \quad (10)$$

where:

$$\varphi = \pi \lambda \varpi. \quad (11)$$

The second step of the derivation models the impact of small-scale fading by defining the r.v.:

$$Q_k = T_k\,\Psi. \quad (12)$$

Since this latter equation identifies a product between r.v.s, the corresponding cdf can be evaluated by applying the product distribution [26], and recalling (5) and (10), thus obtaining:

$$\begin{aligned} F_{Q_k}(q) &= \int_{-\infty}^{+\infty} F_{T_k}\left(\frac{q}{\psi}\right) f_{\Psi}(\psi)\mathrm{d}\psi \\ &= \frac{m^m}{\Gamma(k)\Gamma(m)} \int_0^{+\infty} \Gamma\left(k; \frac{\varphi\psi}{q}\right)\ \psi^{m-1}\exp\left(-m\psi\right)\mathrm{d}\psi \\ &= A_k\,\eta_k(q)\,\mathbb{1}_{\mathbb{R}_{>0}}(q),\ k \in \mathbb{N}_{>0}. \end{aligned} \quad (13)$$

where:

$$A_k = \frac{m^{m-1}\Gamma(k+m)}{\Gamma(k)\Gamma(m)}, \quad (14a)$$

$$\eta_k(q) = \left(\frac{q}{\varphi}\right)^m {}_2F_1\left(m, k+m; m+1; -\frac{mq}{\varphi}\right). \quad (14b)$$

As a third step, consider the effect of mid-scale fading by defining the r.v.:

$$P_k = Q_k\,\Xi, \quad (15)$$

which again denotes a product between r.v.s.. The corresponding cdf $F_{P_k}(p)$ should be hence still derived from the product distribution, now using (4) and (13). This leads to the following integral:

$$\begin{aligned} F_{P_k}(p) &= \int_{-\infty}^{+\infty} F_{Q_k}\left(\frac{p}{\xi}\right)\ f_{\Xi}(\xi)\mathrm{d}\xi \\ &= \frac{A_k}{\sqrt{2\pi}\sigma} \int_0^{+\infty} \frac{1}{\xi}\,\eta_k\left(\frac{p}{\xi}\right)\exp\left(-\frac{\log^2\xi}{2\sigma^2}\right)\mathrm{d}\xi, \end{aligned} \quad (16)$$

which, unfortunately, does not provide a closed-form expression. To overcome this problem, one can exploit the improved Gaussian approximation proposed in [27], which has the advantages of being accurate and computationally light. This approximation, which holds for products involving normal and also log-normal r.v.s, when applied to (16) provides the following result:

$$\begin{aligned} F_{P_k}(p) &\cong \frac{2}{3}\sum_{n=-1}^{1} \frac{1}{4^{|n|}}\,F_{Q_k}\left(\frac{p}{\varepsilon^n}\right) \\ &= \left[\sum_{n=-1}^{1} B_{k,n}\eta_k\left(\frac{p}{\varepsilon^n}\right)\right]\mathbb{1}_{\mathbb{R}_{>0}}(p),\ k \in \mathbb{N}_{>0}, \end{aligned} \quad (17)$$

where:

$$B_{k,n} = \frac{A_k}{3\cdot 2^{2|n|-1}},\ n = -1, 0, 1; k \in \mathbb{N}_{>0}, \quad (18a)$$

$$\varepsilon = \exp(\sqrt{3}\sigma)\,. \quad (18b)$$

The fourth and final step of this analysis is devoted to the calculation of the cdf of the SNR. To this aim, the noise-limited assumption, formulated in [16], is applied. This assumption states that, in a mmWave link, the interference

received by the destination D_k from all the other active nodes different from S may be assumed negligible as long as the antennas are sufficiently directional and the network is not too dense. This implies that the key quantity for estimating the capacity is the SNR, which may be modeled by the r.v.:

$$\Upsilon_k = \frac{P_k}{\mathcal{N}}, \tag{19}$$

where $\mathcal{N}$ represents the constant noise power given by (6). The cdf $F_{\Upsilon_k}(\upsilon)$ of Υ_k may be hence obtained by remembering the scaling rule for r.v.s and then using (17), which leads to:

$$F_{\Upsilon_k}(\upsilon) = F_{P_k}(\mathcal{N}\upsilon) \cong \left[\sum_{n=-1}^{1} B_{k,n}\,\eta_k\left(\frac{\mathcal{N}\upsilon}{\varepsilon^n}\right)\right]\mathbb{1}_{\mathbb{R}_{>0}}(\upsilon),\ k\in\mathbb{N}_{>0}. \tag{20}$$

It is interesting to observe that this cdf is available in analytical form, thus its implementation can be carried out exploiting the numerical routines present in the existing software platforms for the evaluation of the special functions. This reduces the computational time, since the execution of numerical integrations is not necessary.

B. Average capacity

The statistics obtained during the development of the SNR analysis can be properly employed to estimate the average capacity, measured in bits/(s·Hz), which is achievable by the $\mathrm{S}-\mathrm{D}_k$ mmWave communication link in the presence of BPSK and QPSK modulations. To derive this result, one has to preliminarily calculate the average SNR $\mathbf{E}[\Upsilon_k]$. This task might be accomplished by directly integrating the complementary cdf (ccdf) $1-F_{\Upsilon_k}(\upsilon)$, which is immediately inferrable from (20). However, the corresponding integral is rather complex, thus an alternative simpler approach may be preferable. Accordingly, one may recall (12), (15), and (19), to rewrite the r.v. describing the SNR as:

$$\Upsilon_k = \frac{T_k\,\Psi\,\Xi}{\mathcal{N}}, \tag{21}$$

which, by exploiting the independence between T_k, Ψ, and Ξ, leads to:

$$\mathbf{E}[\Upsilon_k] = \frac{\mathbf{E}[T_k]\,\mathbf{E}[\Psi]\,\mathbf{E}[\Xi]}{\mathcal{N}}. \tag{22}$$

This latter expression enables to calculate $\mathbf{E}[\Upsilon_k]$ as the product of three average quantities, which can be separately evaluated. In fact, $\mathbf{E}[T_k]$ may be obtained from the cdf in (10) as:

$$\mathbf{E}[T_k] = \int_0^{+\infty}\left[1-F_{T_k}(t)\right]\mathrm{d}t = \frac{1}{\Gamma(k)}\int_0^{+\infty}\gamma\left(k;\frac{\varphi}{t}\right)\mathrm{d}t = \frac{\varphi}{k-1},\ k\in\mathbb{N}_{>0}-\{1\}, \tag{23}$$

while $\mathbf{E}[\Psi]$ and $\mathbf{E}[\Xi]$ may be derived from the pdfs in (4) and (5), respectively, as:

$$\mathbf{E}[\Psi] = \int_0^{+\infty}\psi f_{\Psi}(\psi)\mathrm{d}\psi = \frac{m^m}{\Gamma(m)}\int_0^{+\infty}\psi^{m-1}\exp\left(-m\psi\right)\mathrm{d}\psi = 1, \tag{24}$$

α (28 GHz)	61.4 dB	W	1 GHz
α (73 GHz)	69.8 dB	$\mathcal{F}$	10
ν	2	P_{S}	100 mW
σ	5.8 dB	G_{S}	10 dB
m	3	G_{D}	10 dB

TABLE I
ADOPTED PARAMETERS [23], [24].

and:

$$\mathbf{E}[\Xi] = \int_0^{+\infty}\xi f_{\Xi}(\xi)\mathrm{d}\xi = \frac{1}{\sqrt{2\pi}\sigma}\int_0^{+\infty}\frac{1}{\xi}\exp\left(-\frac{\log^2\xi}{2\sigma^2}\right)\mathrm{d}\xi = \exp\left(\frac{\sigma^2}{2}\right). \tag{25}$$

By substituting (23), (24), and (25) in (22), one obtains the average SNR as:

$$\mathbf{E}[\Upsilon_k] = \frac{\varphi}{\mathcal{N}(k-1)}\exp\left(\frac{\sigma^2}{2}\right),\ k\in\mathbb{N}_{>0}-\{1\}. \tag{26}$$

The average capacity of the $\mathrm{S}-\mathrm{D}_k$ mmWave link when the BPSK and QPSK modulations are adopted can be finally determined as $C\left(\mathbf{E}[\Upsilon_k]\right)$, by directly using (7). As observed at the end of the previous subsection, also in this case all the derived formulas are available in analytical form, thus their computation can be smoothly carried out.

IV. RESULTS

The numerical values provided by the developed theoretical model are obtained by adopting the parameters reported in Table I, which are inferred from the measurements presented in [24] and [23] carried out in the 28 and 73 GHz bands. In particular, the m value is selected considering the relationship between the Rice factor K and the Nakagami parameter [28]:

$$K = \frac{\sqrt{m^2-m}}{m-\sqrt{m^2-m}}, \tag{27}$$

which, for $m=3$, leads $K\cong 4.45$ ($\cong$6.48 dB). This value is included, in [23], into the experimentally tested LoS scenarios corresponding to the adoption of a vertically polarized antenna at S and a horizontally polarized antenna at D_k. Besides, the intensity of the homogeneous PPP is set from the average cell radius ρ, which is related to λ by [19]:

$$\rho = \frac{1}{\sqrt{\pi\lambda}}. \tag{28}$$

All the results are derived using Matlab and considering a nonuniform discretization of the support of the investigated r.v.s, with the aim of limiting the time required to compute their distributions.

Fig. 1 shows the cdf of the SNR for $\rho = 100$ m and different k values considering the 28 GHz (Fig. 1(a)) and the 73 GHz channels (Fig. 1(b)). Each theoretical curve is validated by Monte Carlo simulations to check the correctness of the analysis and the accuracy of the improved Gaussian approximation in (17). In particular, the numerical values provided by the theory are identified by lines, while those derived from the

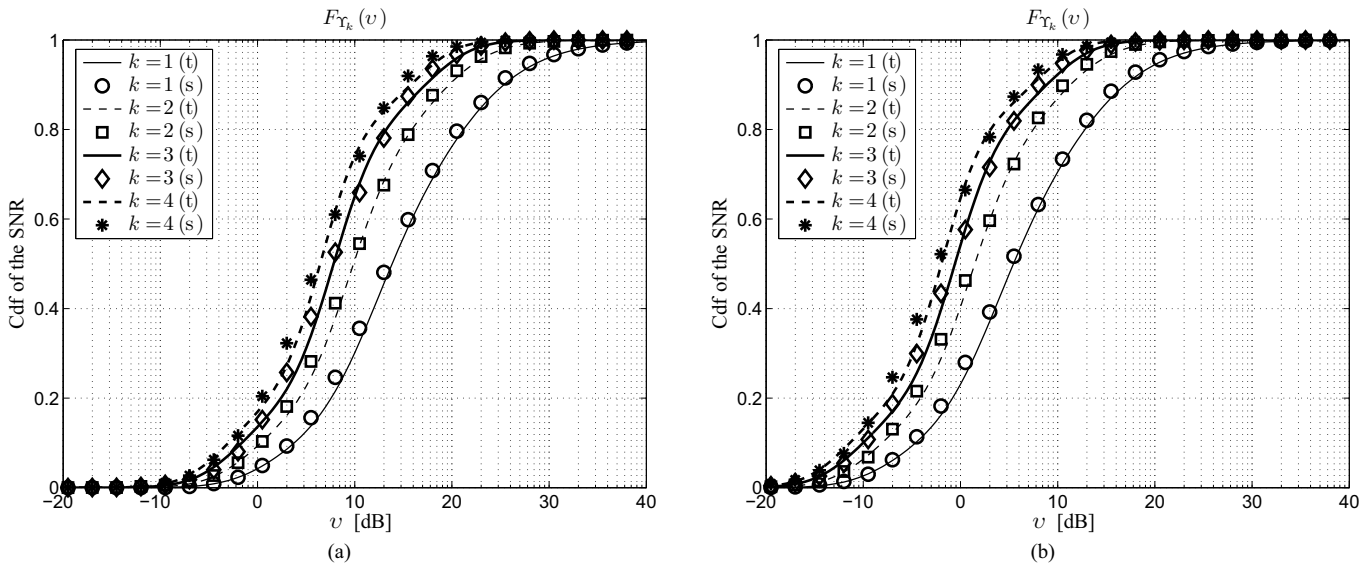

Fig. 1. Theoretical and simulated cdfs of the SNR for $\rho = 100$ m: (a) 28 GHz channel, (b) 73 GHz channel (t: theory, s: Monte Carlo simulation).

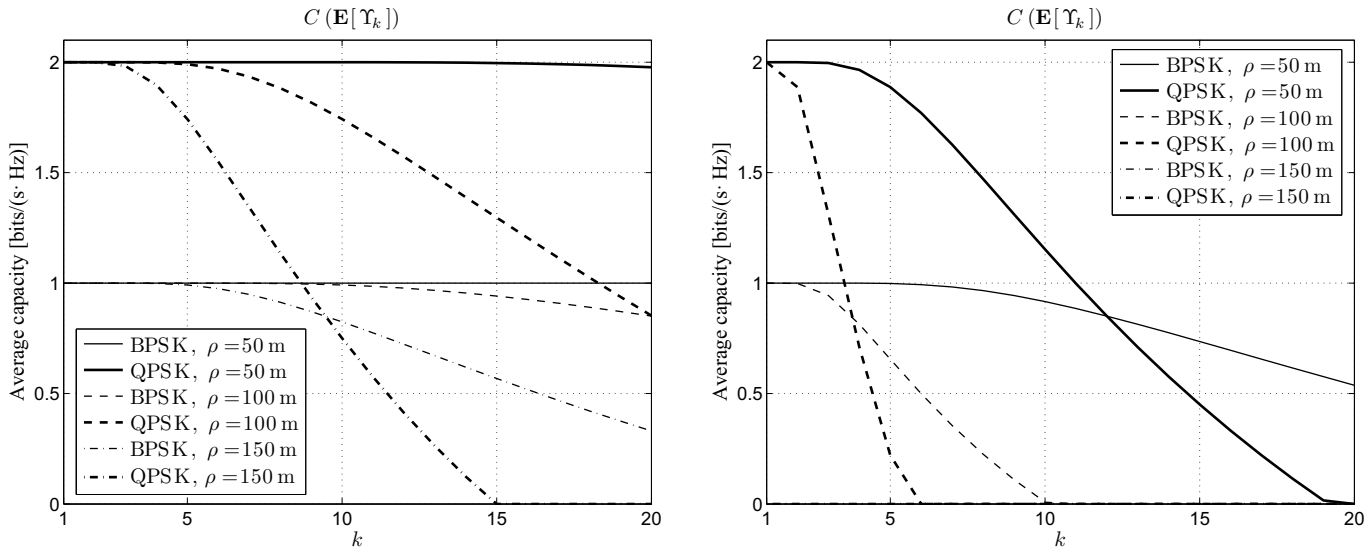

Fig. 2. Average capacity as a function of the neighbor's order for different average cell radii when the BPSK and QPSK modulations are adopted: (a) 28 GHz channel, (b) 73 GHz channel.

simulations, obtained by running $M = 100000$ realizations for each point, are represented by markers. One may immediately note the considerable matching between theory and validation, which suggests a satisfactory reliability of the developed analysis. From the technical point of view, Fig. 1 confirms that a higher SNR is statistically achievable at the lower frequency band, since the 73 GHz one is characterized by a higher path-loss (Table I). A reduction of the SNR may be also observed as far as the order of the neighbor increases. In fact, for a given mmWave band, the best performance is obtained when $\mathrm{D}_k = \mathrm{D}_1$, that is, when the destination location coincides with the nearest neighbor. For the subsequent neighbors, the higher the k value the higher the probability that the SNR be lower than a given threshold. This behavior is due to the expected higher $\mathrm{S} - \mathrm{D}_k$ distance when k increases. However, the performance decrease becomes less significant with the increase of k itself. In fact, one may observe that the difference $F_{\Upsilon_{k-1}}(\upsilon) - F_{\Upsilon_k}(\upsilon)$ gets lower as $k(\geq 2)$ gets higher.

Fig. 2 illustrates the average capacity as a function of the neighbor's order for different average cell radii when the BPSK and QPSK modulations are employed, still considering the 28 GHz (Fig. 2(a)) and the 73 GHz channels (Fig. 2(b)). In this figure, the simulations are not reported, since $C(\mathbf{E}[\Upsilon_k])$ directly depends on the average SNR and hence on $F_{\Upsilon_k}(\upsilon)$, whose accuracy has been already checked in the previously discussed set of results. Besides, as a preliminary observation, it is worth to remark that, when the BPSK modulation is adopted, the maximum achievable capacity is equal to one, while, when the QPSK modulation is used, the maximum capacity is equal to two. Therefore, Fig. 2 reveals that the

expected capacity reduction when k increases is substantially absent for small cells ($\rho = 50$ m) in the 28 GHz channel. The opposite case, in which none of the two modulations is sustainable, occurs for large cells ($\rho = 150$ m) in the 73 GHz channel (the corresponding dash-dotted curves in Fig. 2(b) coincide with the k-axis and are hence not visible). In the other cases, an intermediate performance is achieved, with the average capacity that decreases with the increase of the neighbor's order and of the frequency channel. In particular, it is interesting to observe that, in the 28 GHz channel, even a statistically very far destination (i.e., D_{20} for $\rho = 150$ m) can be served at a fraction of the basic rate supported by the BPSK modulation. This means that, in LoS conditions, a low-capacity link can be established at the boundary of large cells when the selected mmWave band is not too high. However, in general, the figure suggests that small cells are preferable, since they lead to higher capacity values, even if cells of medium size ($\rho = 100$ m) can anyway provide an acceptable performance in the 28 GHz channel. A similar behavior may be observed for the other m values leading, by (27), to the Rice factors lying between 0 and 7 dB, corresponding to the interval experimentally derived in [23].

V. Conclusions

A PPP-based theoretical model for calculating the cdf of the SNR and the average capacity of a source-destination mmWave LoS communication has been presented. The analysis has been used to study the influence of the average cell radius and of the mmWave band on the link performance when the destination can be a neighbor of any order. Path-loss attenuation, mid- and small-scale fading, together with BPSK/QPSK modulations have been included in the developed model, deriving closed-form expressions for the quantities of interest. The results have shown that the neighbor's order has a significant influence on the link capacity, even if the performance reduction between two consecutive orders decreases when they increase. Concerning the selection of the frequency band, it has been observed that the 28 GHz channel can guarantee an acceptable performance also for statistically far destinations until the average cell radius is not too high. Current research efforts aim to extend the proposed analysis to the NLoS scenario with the aim of characterizing the mmWave communication in any channel state.

References

[1] J.G. Andrews, S. Buzzi, W. Choi, S.V. Hanly, A. Lozano, A.C.K. Soong, and J.C. Zhang, "What will 5G be?" *IEEE J. Sel. Areas Commun.*, vol. 32, no. 6, pp. 1065–1082, June 2014.

[2] A. Seetharaman, N. Niranjan, V. Tandon, S. Devarajan, M.K. Moorthy, and A.S. Saravanan, "What do customers crave in mobile 5G? A survey spotlights four standout factors," *IEEE Consum. Electron. Mag.*, vol. 6, no. 3, pp. 52–66, July 2017.

[3] T.S. Rappaport, S. Sun, R. Mayzus, H. Zhao, Y. Azar, K. Wang, G.N. Wong, J.K. Schulz, M. Samimi, and F. Gutierrez, "Millimeter wave mobile communications for 5G cellular: It will work!" *IEEE Access*, vol. 1, pp. 335–349, May 2013.

[4] F. Babich and M. Comisso, "Impact of segmentation and capture on slotted Aloha systems exploiting interference cancellation," *IEEE Trans. Veh. Technol.*, vol. 68, no. 3, pp. 2878–2892, Mar. 2019.

[5] K. Cengiz and M. Aydemir, "Next-generation infrastructure and technology issues in 5G systems," *J. Commun. Soft. Syst.*, vol. 14, no. 1, pp. 33–39, Mar. 2018.

[6] J.G. Andrews, T. Bai, M.N. Kulkarni, A. Alkhateeb, A.K. Gupta, and R.W. Heath Jr., "Modeling and analyzing millimeter wave cellular systems," *IEEE Trans. Commun.*, vol. 65, no. 1, pp. 403–430, Jan. 2017.

[7] M. Comisso, G. Palese, F. Babich, F. Vatta, and G. Buttazzoni, "3D multi-beam and null synthesis by phase-only control for 5G antenna arrays," *Electronics*, vol. 8, no. 6, p. 13, June 2019, Article ID656.

[8] W. Hong, Z.H. Jiang, C. Yu, J. Zhou, P. Chen, Z. Yu, H. Zhang, B. Yang, X. Pang, M. Jiang, Y. Cheng, M.K.T. Al-Nuaimi, Y. Zhang, J. Chen, and S. He, "Multibeam antenna technologies for 5G wireless communications," *IEEE Trans. Antennas Propag.*, vol. 65, no. 12, pp. 6231–6249, Dec. 2017.

[9] M. Comisso, "On the use of dimension and lacunarity for comparing the resonant behavior of convoluted wire antennas," *Progr. Electromag. Res., PIER 96*, pp. 361–376, 2009.

[10] P. Schulz, M. Matthé, H. Klessig, M. Simsek, G. Fettweis, J. Ansari, S.A. Ashraf, B. Almeroth, J. Voigt, I. Riedel, A. Puschmann, A. Mitschele-Thiel, M. Müller, T. Elste, and M. Windisch, "Latency critical IoT applications in 5G: Perspective on the design of radio interface and network architecture," *IEEE Commun. Mag.*, vol. 55, no. 2, pp. 70–78, Feb. 2017.

[11] R. Corrado, M. Comisso, and F. Babich, "On the impact of the video quality assessment in 802.11e ad-hoc networks using adaptive retransmissions," in *IEEE IFIP Med-Hoc-Net*, 2014.

[12] G.A. Akpakwu, B.J. Silva, G.P. Hancke, and A.M. Abu-Mahfouz, "A survey on 5G networks for the Internet of Things: Communication technologies and challenges," *IEEE Access*, vol. 6, pp. 3619–3647, Feb. 2018.

[13] K.C-J. Lin, S. Gollakota, and D. Katabi, "Random access heterogeneous MIMO networks," in *ACM SIGCOMM Conf.*, 2011.

[14] F. Babich, M. Comisso, and A. Dorni, "A novel SIR-based access scheme for multi-packet communication in 802.11 networks," in *IEEE ICC*, 2012.

[15] S. Selmi and R. Bouallègue, "Spectral and energy efficient D2D communication underlay 5G networks: A mixed strategy approach," *J. Commun. Soft. Syst.*, vol. 16, no. 1, pp. 57–65, Mar. 2020.

[16] S. Singh, R. Mudumbai, and U. Madhow, "Interference analysis for highly directional 60-GHz mesh networks: The case for rethinking medium access control," *IEEE/ACM Trans. Netw.*, vol. 19, no. 5, pp. 1513–1527, Oct. 2011.

[17] T. Bai and R.W. Heath Jr., "Coverage and rate analysis for millimeter-wave cellular networks," *IEEE Trans. Wireless Commun.*, vol. 14, no. 2, pp. 1100–1114, Feb. 2015.

[18] F. Babich and M. Comisso, "Multi-packet communication in heterogeneous wireless networks adopting spatial reuse: Capture analysis," *IEEE Trans. Wireless Commun.*, vol. 12, no. 10, pp. 5346–5359, Oct. 2013.

[19] M. Di Renzo, "Stochastic geometry modeling and analysis of multi-tier millimeter wave cellular networks," *IEEE Trans. Wireless Commun.*, vol. 14, no. 9, pp. 5038–5057, Sep. 2015.

[20] H. Shokri-Ghadikolaei, C. Fischione, G. Fodor, P. Popovski, and M. Zorzi, "Millimeter wave cellular networks: A MAC layer perspective," *IEEE Trans. Commun.*, vol. 63, no. 10, pp. 3437–3458, Oct. 2015.

[21] H.R. Thompson, "Distribution of distance to nth neighbour in a population of randomly distributed individuals," *Ecology*, vol. 37, no. 2, pp. 391–394, Apr. 1956.

[22] M. Grossglauser and D.N.C. Tse, "Mobility increases the capacity of ad hoc wireless networks," *IEEE/ACM Trans. Netw.*, vol. 10, no. 4, pp. 477–486, Aug. 2002.

[23] M.K. Samimi, G.R. MacCartney Jr., S. Sun, and T.S. Rappaport, "28 GHz millimeter-wave ultrawideband small-scale fading models in wireless channels," in *IEEE VTC Spring*, 2016.

[24] M.R. Akdeniz, Y. Liu, M.K. Samimi, S. Sun, S. Rangan, T.S. Rappaport, and E. Erkip, "Millimeter wave channel modeling and cellular capacity evaluation," *IEEE J. Sel. Areas Commun.*, vol. 32, no. 6, pp. 1164–1179, June 2014.

[25] F. Babich, A. Soranzo, and F. Vatta, "Useful mathematical tools for capacity approaching codes design," *IEEE Commun. Lett.*, vol. 21, no. 9, pp. 1949–1952, Sep. 2017.

[26] R.D. Yates and D.J. Goodman, *Probability and Stochastic Processes*. Ed. New York: Wiley, 1999.

[27] J.M. Holtzman, "A simple, accurate method to calculate spread-spectrum multiple-access error probabilities," *IEEE Trans. Commun.*, vol. 40, no. 3, pp. 461–464, Mar. 1992.

[28] G.L. Stuber, *Principles of mobile communication*. Norwell MA, Kluwer Academic Publishers, 1996.